X-RAY STRUCTURE ANALYSIS OF THIN FILAMENTS OF A MOLLUSCAN SMOOTH MUSCLE IN THE LIVING RELAXED STATE

YOSHIKO TAJIMA, KIYOSHI KAMIYA, AND TSUNEO SETO
Department of Physics, Tokyo Metropolitan University, Setagaya-ku, Tokyo, Japan 158

ABSTRACT In the small-angle x-ray diffraction pattern of the living relaxed anterior byssus retractor muscle of *Mytilus edulis*, the thin filaments showed the following features. The 59.8-Å reflection was much stronger and a little farther from the meridian than the 51.9-Å reflection, although they are both contributions of the first-order Bessel function and are comparable with each other in the height from the equator. The 381-Å reflection, given by the second-order Bessel function, was weaker than the 59.8-Å reflection by more than the difference between the peak values of the first- and second-order Bessel functions, and was not so distant radially from the latter as estimated from the amount of peak shift brought about by the alteration of the Bessel order. A model of the thin filament was made on the basis of inverse Fourier transformation of the scattering amplitude, and the above features were explained by the characteristic shape of actin shown in this model. The actin subunits are elongated along the genetic left-hand helix with a pitch of 59.8 Å, and are bonded together along the genetic helix in the inner part of the filament.

INTRODUCTION

The thin actin-containing filament plays one of the leading roles in muscle contraction, and many studies have been carried out to clarify the structure of the filament. Hanson and Lowy (1963) presented the helical arrangement of actin molecules, and made suggestions on the location of a regulatory protein, tropomyosin. Ohtsuki et al. (1967) demonstrated the regular arrangement of another regulatory protein, troponin. On the basis of these studies Ebashi (1972) proposed a model of the thin filament.

The arrangement of molecules given by Ebashi has been supported by small-angle x-ray diffraction of a variety of muscles. It seems, however, that this model is primarily intended to show the disposition of the constituent proteins of the filament, since actin, tropomyosin, and troponin are simply represented by a sphere, a solid cylinder, and a flat ellipsoid, respectively. Therefore, the features of the small-angle x-ray diffraction pattern attributable to the shape of the proteins, especially actin, are still unexplained. For detailed explanation of the intensities and positions of the reflections, it is necessary to determine the shape of the constituent proteins more precisely. For understanding the mechanism of the interaction between the thin and thick filaments at muscle contraction, it is helpful to know the shape of the molecules in the filaments.

In this work, the shape of actin was studied by inverse Fourier transformation of the scattering amplitude under the assumption that it was nonpolar, and it was shown that some distinctive features of the small-angle x-ray diffraction pattern of the thin filaments were brought about by the characteristic shape of actin. The specimen of this work was the anterior byssus retractor muscle of *Mytilus edulis* (ABRM) in the living relaxed state. The thin filaments of this muscle are ~10 times as long as those of vertebrate striated muscle (Sobieszek, 1973), and do not contain troponin (Lehman et al., 1972). Therefore, the ABRM produces a clear and strong x-ray pattern from the thin filaments (Vibert et al., 1972 *a, b*; Lowy and Vibert, 1972) that appears simple because of the lack of the reflection from troponin, and is advantageous for structure analysis of the actin helix.

Wakabayashi et al. (1975) proposed a model of the thin filament in the inhibited state by three-dimensional image reconstruction from electron micrographs. The model was cut out from the density map at high density to show the relatively reliable features of the structure. In this model the polar actin subunits are bonded together along the left-hand helix with a pitch of 59 Å at the bonding sites located in the inner side of the actin subunits. Aebi et al. (1981) made image processing of electron micrographs of crystalline sheets of actin, and obtained a model of the actin molecule in projection having resemblance to the actin subunit in the model of Wakabayashi et al., but they proposed an orientation of the molecules in the actin filament different from that in the latter model. Suck et al. (1981) carried out x-ray structure analysis of the single crystals of actin complexed with bovine pancreatic DNase I, and determined the shape and dimensions of the actin molecule. However, it was concluded that the contact between actin molecules in the crystal was different from the contact in the actin filament.

MATERIALS AND METHODS

The ABRM, ~25-mm long and 1-mm thick, was obtained from an animal ~70- mm long. The ABRM was dissected by the method of Jewell (1959) and Vibert et al. (1972 *b*), relaxed by 5-hydroxytriptamine (Twarog, 1960), and set at rest length (Lowy and Millman, 1963) in the specimen chamber made of acrylic resin. For the purpose of checking that the muscle was in the relaxed state without producing tonic tension (Lowy and Millman, 1963), one end of the muscle was tied to an acrylic lever transmitting the tensile force to a strain gauge. Aerated artificial sea water of the composition given by Millman (1964) flowed slowly and incessantly through the specimen chamber maintained at 5°C.

X-ray diffraction patterns were taken by an x-ray apparatus (Rigaku Denki, Inc., Tokyo, Japan), a rotating anode microfocusing x-ray generator operated at 40 kV and 15 mA (nominal focal size 0.1 mm × 0.1 mm), and a mirror monochromator point focusing camera with 3°-cut quartz crystal as monochromator. The x-ray patterns were recorded on Sakura Cosmic-Ray Ester film (Rokuo Shoji, Inc., Tokyo, Japan) of factor 2.88. The diffraction pattern was simultaneously recorded on five films packed in layers in the film cassette. The distance between the specimen and the film was 19 cm, and the exposure time 96 h. The ABRM was maintained for a long period of time in the living state in the specimen chamber, and lasted through this long-time exposure. Some specimens were stimulated by alternating current every 5 h after the dissection, and after 90 h, the specimens still produced 80% of the tension obtained at the first stimulation.

Intensities of the layer-line reflections were measured by microphotometer by the method of Namba et al. (1980). The slit size was 20 μm × 50 μm. Scanning was done perpendicularly to the layer line at intervals of 0.3 mm corresponding to 0.001 $Å^{-1}$. Since the orientation of the filaments was not perfect, the layer-line reflections gradually became broader with increasing distance from the meridian. Therefore, after subtraction of the background intensity, the area under the peak corresponding to the integral intensity was measured and plotted as a function of the distance from the meridian to obtain the intensity profiles along the layer lines.

RESULTS

For measuring accurately the intensities of the layer-line reflections, it is important to obtain x-ray diffraction patterns showing good orientation of the filaments. Ten diffraction patterns were taken, and the one showing the best orientation of the thin filaments was chosen for structure analysis (Fig. 1). The layer-line reflections from the thin filaments are schematically shown in Fig. 2. The reciprocal axial coordinates, Z_i, of the layer lines and the spacings, d_i, corresponding to them are shown in Table I. On the equator, broad diffraction spots appeared at (128 $Å)^{-1}$ associated with the sideways packing of the thin filaments (Elliott and Lowy, 1968).

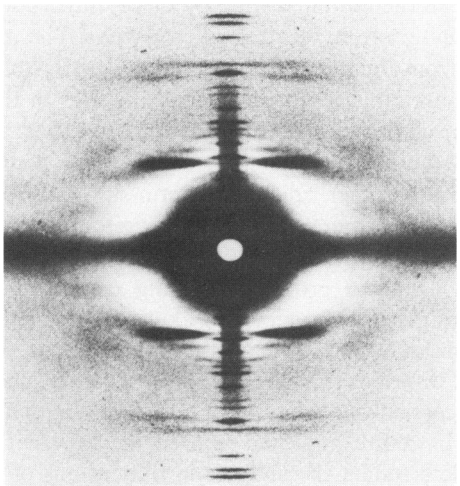

FIGURE 1 Small-angle x-ray diffraction pattern of the living relaxed ABRM. The pattern was reproduced by a background leveling technique (Vibert et al., 1972 *b*) to improve the visibility of the weak reflections.

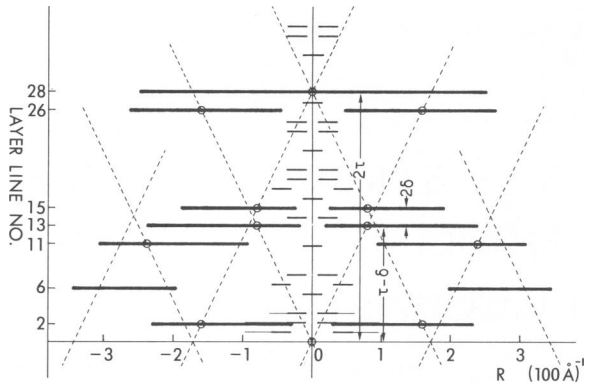

FIGURE 2 Schematic diagram of the layer line reflections from the thin and thick filaments in the pattern shown in Fig. 1. The long bold lines (—) represent the reflections from the thin filaments and the layer lines are numbered on the left side. The fine broken lines (---) show the arrangement of the reflections into a set of oblique crosses given by a discontinuous helix of pitch 59.8 Å and axial subunit repeat 27.8 Å. The reflection on the 6th layer line is so near to the meridian as to be out of this arrangement, because this reflection is given by the tropomyosin helices, which have a larger diameter than the actin helix (Vibert et al., 1972 *b*). The broad reflection seen in Fig. 1 just outside the reflection on the 11th layer line at almost the same axial distance from the equator as the 13th and 15th layer lines can not be indexed by the same indexing scheme with the layer lines from the thin filaments. It is probably reflection from paramyosin molecules composing the cores of the thick filaments. The thin short lines (— —) on and near the meridian represent reflections from the thick filaments.

The reflections shown by the thin lines on and near the meridian in Fig. 2 are from the thick filaments (mostly from the paramyosin core). Off-meridional reflections showing helical arrangement of the myosin heads were not observed. Because the thick filaments of the ABRM have very large diameters (Sobieszek, 1973), the myosin heads

TABLE I
OBSERVED LAYER LINES FROM THE THIN FILAMENTS

Identification number i	Axial coordinate Z_i ($\times 10^{-3}$)	Spacing d_i	Layer-line number l	Bessel order n	$l \times d_i$
	$Å^{-1}$	Å			Å
1	2.63	381	2	2	762
2	7.60	131.6	6	6	790
3	14.16	70.6	11	−3	777
4	16.71	59.8	13	−1	777
5	19.25	51.9	15	1	779
6	33.37	30.0	26	−2	780
7	35.88	27.9	28	0	781

probably form a helical lattice with a high-order circular symmetry (Squire, 1973), so that they only produce very weak reflections in the off-meridional region given by high-order Bessel functions (Wray et al., 1975). Because the filaments taper off, the order of the circular symmetry changes along the filament. This change also makes the reflections indistinct.

It is probable that the thin filaments are not integral helices, and the layer lines from the thin filaments shown in Fig. 2 do not have integral indices (Vibert et al., 1972 *b*; Maeda et al., 1979). For convenient description and analysis of structure, however, we assumed an integral helical symmetry fitted all the layer lines. It was determined from the ratio of the pitch of the genetic helix C against the axial repeat of actin c' obtained in the following way.

According to the general diffraction theory of helix (Vainshtein, 1966), reflections from a discontinuous helix, which is a system of helically arranged points, are arranged into a set of oblique crosses; that is, a cross at the origin given by a continuous helix having the same pitch as the discontinuous helix and the identical crosses translated along the meridian by integral multiples of the reciprocal of the axial subunit repeat. Therefore, the axial coordinates of the layer lines from the thin filaments were expressed as functions of Z_4 and Z_7 corresponding to C and c', respectively (Fig. 2). Replacing Z_4 and Z_7 with $\tau - \delta$ and 2τ, respectively, we obtained $Z_1 = 2\delta$, $Z_2 = 6\delta$, $Z_3 = \tau - 3\delta$, $Z_5 = \tau + \delta$, and $Z_6 = 2(\tau - \delta)$. By substitution of the observed axial coordinates into the equations $Z_1 = 2\delta$, $Z_6 = 6\delta$, $Z_4 - Z_3 = 2\delta$, $Z_5 - Z_4 = 2\delta$, and $Z_7 - Z_6 = 2\delta$, five values of δ were obtained. By averaging them $\bar{\delta} = 1.274 \times 10^{-3}$ Å^{-1} was obtained. Similarly, we obtained τ for each of the layer lines from $i = 3$ to $i = 7$ by substitution of $\bar{\delta}$ into δ, and $\bar{\tau} = 17.96 \times 10^{-3}$ Å^{-1} was given. Then $C/c' = 2\bar{\tau}/(\bar{\tau} - \bar{\delta}) = 2.153 \approx 28/13$. Therefore, the filament had a helical symmetry of 28/13, that is, 13 turns of the genetic helix and 28 subunits were included in one structural period. The indices of the layer lines and the orders of the Bessel functions were determined from this symmetry (Table I). The pitch of the genetic helix C, and the axial repeat of actin c', and the structural period c were on an average 59.8 Å, 27.8 Å, and 778 Å, respectively. The scattering of the structural periods given from all the layer lines, $l \times d_l$ (Table I), about the mean value is within 2.1% of the mean value. The helical symmetry 28/13 delineates the structure of the thin filament in good approximation, and was used in this work.

Fig. 3 *a* shows the intensity profiles of the thin filaments obtained by densitometry of the diffraction photograph. Lattice-sampling effect was not observed on any layer line. These profiles are equivalent to the cylindrically averaged diffraction intensities from one isolated thin filament. In

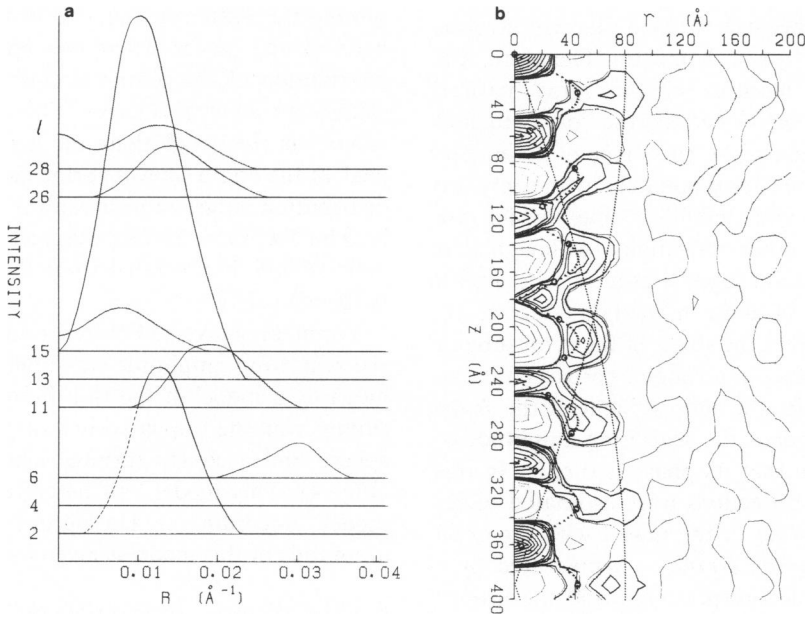

FIGURE 3 (*a*) Intensity profiles of the layer-line reflections from the thin filaments in the pattern shown in Fig. 1. Because the 2nd layer line from the paramyosin cores of the thick filaments was very strong, and extended as far as 0.01 Å^{-1}, the intensity of the 2nd layer line from the thin filaments could not be measured for the radial coordinate $R < 0.01$ Å^{-1}, and the intensity profile was extrapolated into this range (---). (*b*) Contour map of the cylindrically symmetrical difference Patterson function obtained by Fourier transformation of the intensities shown in *a*. The peak at the origin was normalized to 1,000. The thick lines (—) are positive contour lines of 5, 20, 50, 70, 100, 200, 300, etc., and the thin lines (—) are zero and negative contour lines with intervals of 100. The dotted line (· · ·) curved periodically along the *z*-axis is the Patterson function of a continuous helix with a pitch of 59.8 Å passing approximately through the centers of the actin subunits; that is, the locus of the genetic helix. The open circles (O) on this dotted line show the distribution of the distance between the actin subunits. The two gently curved dotted lines (· · ·) are the Patterson function of a continuous double helix with a radius of 40 Å representing approximately the loci of the tropomyosin strands.

this figure the ABRM shows the following features that, having been observed in other muscles (Namba et al., 1980; Wray et al., 1978), appear to indicate general structural features of the thin filament. (*a*) The reflection on the 13th layer line is much stronger and a little farther from the meridian than the reflection on the 15th layer line, although these reflections are both contributions of the first-order Bessel function and are comparable with each other in the height from the equator. (*b*) The reflection of the 2nd layer line, given by the second-order Bessel function, is weaker than the reflection on the 13th layer line by more than the difference between the peak values of the first- and second-order Bessel functions, although the former is nearer to the origin than the latter. The former is also not so distant radially from the latter as estimated from the amount of peak shift of the Bessel function at the change of the Bessel order. This work was carried out to explain these features.

STRUCTURE ANALYSIS

Outline of the Method of Structure Analysis

Because the tropomyosin strands form approximately continuous helices making one turn in one structural period, they do not contribute to the reflections except on the 2nd and 6th layer lines (Haselgrove, 1972). The intensity on the 2nd layer line is also determined predominantly by the contribution from actin, because the thin filament involves much less mass of tropomyosin than actin. Therefore, it is thought that the two features of the x-ray pattern described in the last section concerning the 2nd, 13th, and 15th layer lines are explained by the shape of actin. The shape of actin is determined approximately by the only two reflections on the 13th and 2nd layer lines, which are distinctly stronger than other reflections. Although it is shown in the model of Wakabayashi et al. (1975) and is inferred from the shape of actin in crystals (Aebi et al., 1981; Suck et al., 1981) that the shape of the actin subunit is polar, it appears possible, in a rough approximation, to adopt a nonpolar model for the actin subunit. If the shape of actin is assumed nonpolar, the scattering amplitude of the actin helix is real, so that its phase is 0 or π. In this work, the phases of the reflections were estimated under this assumption by referring to the model with the actin subunit and the tropomyosin strand as represented by a sphere and a solid cylinder, respectively, and the inverse Fourier transformation of the scattering amplitude, given by the combination of the estimated phase and the square root of the observed intensity, was carried out. A new model of the thin filament was made on the basis of the inverse Fourier transformation.

The cylindrically averaged scattering intensity on the lth layer line per one structural period is given by

$$I_l(R) = \sum_n |G_{nl}(R)|^2, \tag{1}$$

where

$$G_{nl}(R) = \int_0^\infty g_{nl}(r) J_n(2\pi Rr) \cdot 2\pi r dr, \tag{2}$$

and

$$g_{nl}(r) = (q/2\pi) \int_0^\infty \int_0^{2\pi} \rho_0(r, \phi, z) \cdot \exp[-i(n\phi - 2\pi lz/c)] d\phi dz. \tag{3}$$

Here, (r, ϕ, z) and (R, Φ, Z) are cylindrical coordinates in the real and reciprocal spaces, and the z-axis is parallel to the axis of helical symmetry. The function $\rho_0(r, \phi, z)$ is the electron density of one subunit, and q is the number of the subunits in one structural period c.

Each of the observed layer-line reflections from the thin filaments corresponding to the first term of the sum in Eq. 1. The absolute value of $G_{nl}(R)$ is given by the square root of the observed intensity. If the structure of the subunit is nonpolar, $\rho_0(r, \phi, z)$ is even with respect to ϕ and z, that is $\rho_0(r, -\phi, -z) = \rho_0(r, \phi, z)$. Then, both $g_{nl}(r)$ and $G_{nl}(R)$ are real, and the phase of $G_{nl}(R)$ is 0 or π.

Inverse Fourier Transformation

Fig. 3 *b* shows the cylindrically symmetrical difference Patterson function (Namba et al., 1980) obtained by Fourier transformation of the intensities shown in Fig. 3 *a*. The positive contour lines extend along the curve representing the Patterson function of the locus of the genetic helix at the places where the open circles showing the distribution of the actin subunits are relatively close to each other along this curve. This indicates that the actin subunit is elongated along the genetic helix. The positive peak at the origin showing principally the internal distance distribution of one actin subunit is flat and extends radially. This fact can also be explained by considering that the actin subunit is elongated along the genetic helix, and thin perpendicularly.

For making inverse Fourier transformation, the phase of the scattering amplitude was approximated by the phase given by a model of the thin filament in which the actin subunit and the tropomyosin strand were represented by a sphere and a slowly turning solid cylinder, respectively (Fig. 4). This model will hereafter be called the sphere model. According to Haselgrove (1972), the scattering amplitude of this model is given by

$$G_{nl}(R) = \{3(\sin x - x\cos x)/x^3\} J_n(2\pi R r_A) + W_{TM}\{2J_1(2\pi R r_{0T})/(2\pi R r_{0T})\} J_l(2\pi R r_T) \exp(-il\psi), \tag{4}$$

where

$$x = 2\pi r_{0A}\{R^2 + (l/c)^2\}^{1/2}, \tag{5}$$

and r_{0A}, r_A, r_{0T}, and r_T are the radii of actin, the helix of actin, the tropomyosin strand, and the helix of tropomyosin, respectively. It was shown by Haselgrove (1972) that

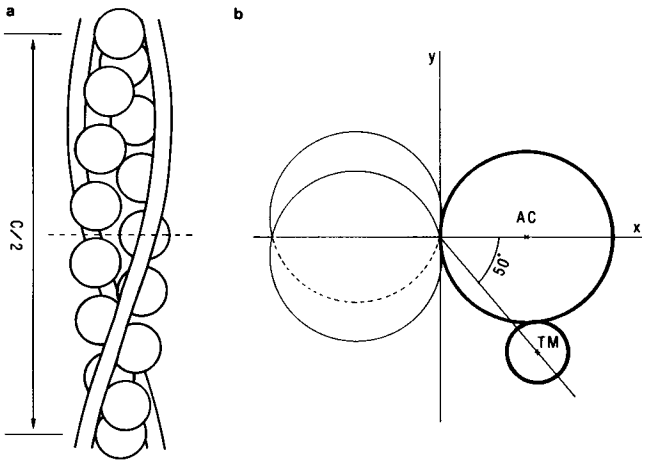

FIGURE 4 Sphere model of the thin filament in the relaxed state. The cross section of one subunit as indicated by the broken line (— —) in *a* and by the bold lines (——) in *b*.

the azimuthal angle of the tropomyosin strand, ψ, is 50° in the relaxed state (Fig. 4 *b*). The coefficient, W_{TM}, is the ratio of the weight of tropomyosin to the weight of actin involved in one structural period, and is equal to 0.23 for the 28/13 helix with actin molecules of weight 42,000 (Elzinga et al., 1973), and tropomyosin molecules of weight 67,000 (Woods, 1969).

Fig. 5 *a* shows the layer-line intensities from the sphere model calculated by substitution of $r_{0A} = r_A = 24$ Å, $r_{0T} = 8.5$ Å, and $r_T = 42.2$ Å into Eq. 4. The phase of the reflection is π on the 11th, 13th, 26th, and 28th layer lines, 0 on the 15th layer line, and 23.4° and −58.2° at the peaks on the 2nd and 6th layer lines, respectively. The scattering amplitude on the lth layer line from the thin filaments of the ABRM was given in the form

$$G_{nl}(R) = \{I_l(R)\}^{1/2}\exp\{i\alpha_l(R)\} \qquad (6)$$

by approximation of the phase $\alpha_l(R)$ with that of the reflection from the sphere model. Here $I_l(R)$ is the observed intensity on the lth layer line.

Fig. 6 shows contour maps of the inverse Fourier transform of the scattering amplitude involving all the observed layer lines, each of which is given by Eq. 6. The areas corresponding to actin and the tropomyosin strand are well recognized by the contour lines of 10% of the highest peak value. The small positive peaks in the third quadrant and at the left side of the second quadrant of Fig. 6 *a* are considered the false peaks formed by the use of the approximate phase. Fig. 6 *b* shows that actin is elongated along the genetic helix.

Because the reflections on the equator were not involved, the inverse Fourier transform corresponds to the deviation of the electron density $\rho(\mathbf{r})$ from its z-average, $\Delta\rho(\mathbf{r})$. Because $\rho(\mathbf{r})$ is taken to be constant in small angle x-ray diffraction, $\Delta\rho(\mathbf{r})$ is positive inside the molecules, and the boundaries between the positive and negative areas indicate the shape of the molecules. However, because of the termination effect; that is, the reflections at higher scattering angles being omitted at the inverse Fourier transformation, the zero contour lines must be shifted from the lines indicating the shape of the molecules. The amount of shifting was estimated by comparison of the sphere model with the inverse Fourier transform of the calculated scattering amplitude of the sphere model involving only the reflections corresponding to the observed ones. By the help of this estimation, the lines showing the shape of actin were

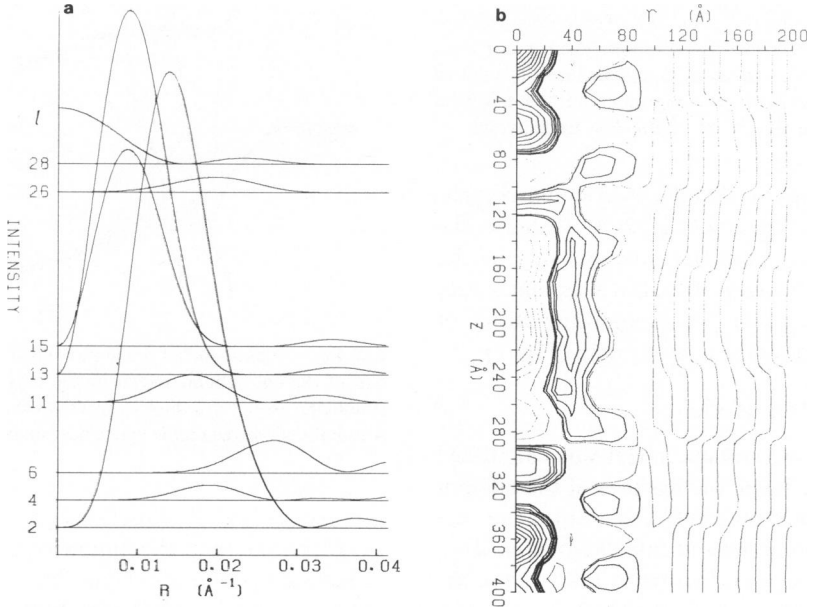

FIGURE 5 (*a*) Cylindrically averaged intensities calculated for the model shown in Fig. 4. (*b*) Cylindrically symmetrical difference Patterson function obtained by Fourier transformation of the intensities shown in *a*. The same contour lines as in Fig. 3 *b* are used.

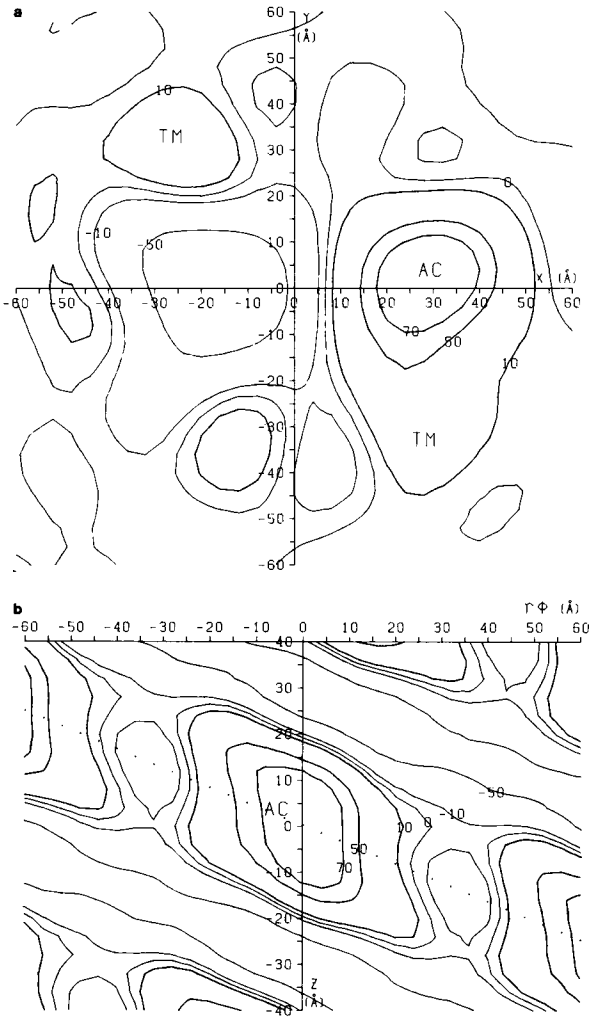

FIGURE 6 Contour maps of the inverse Fourier transform of the scattering amplitude. (*a*) Cross section passing through the center of the actin subunit. (*b*) Cylindrical section at radius 23 Å. The highest peak in *a* was normalized to 100. The thick lines (——) are positive contour lines, and the thin lines (——) are zero and negative contour lines. The dotted straight line (· · ·) in *b* represents the projection of the left-hand continuous helix with a pitch of 59.8 Å. *AC*: actin; *TM*: tropomyosin.

drawn in the contour maps on the planes oriented perpendicularly to the *z*-axis at intervals of 2 Å. Because the resolution is not high enough to determine the shape of the cross section of the tropomyosin strand, it was tentatively represented by a circle of radius 8.5 Å, and the position of the circle was determined by the contour map (Fig. 7).

Correction of the Model

The scattering intensity of the new model was calculated numerically by Eqs. 1–3. Then, the features of the diffraction pattern in question appeared. For improving the agreement between the observed and calculated intensities, a little change of the model was iterated by referring to the value of $2\pi r g_{nl}(r)$. Eq. 2 shows that the change in the structure affects the change in the intensity through $g_{nl}(r)$. The scattering amplitude $G_{nl}(R)$ is taken for the sum of the

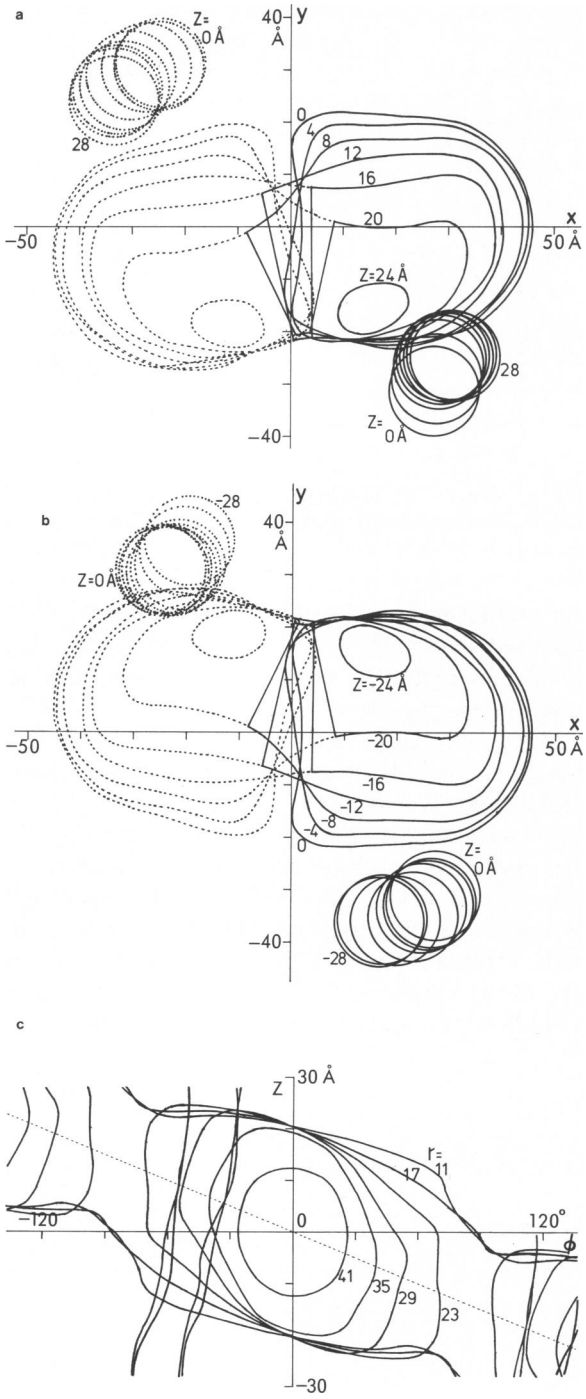

FIGURE 7 New model of the thin filament. (*a*) Upper half and (*b*) lower half of the one subunit shown by the cross sections at intervals of 4 Å (solid lines, ——). (*c*) Cylindrical sections at radii 11, 17, 23, 29, 35, and 41 Å radially projected on the cylindrical surface at radius 23 Å.

nth-order Bessel functions $J_n(2\pi Rr)$ weighted with $2\pi r g_{nl}(r)$, so that the intensity and the position of the reflection on the *l*th layer line are determined by the magnitude of $2\pi r g_{nl}(r)$ as a function of r. The reciprocal radial coordinate R at which the Bessel function, $J_n(2\pi Rr)$, has a maximum is inversely proportional to r, that is, $R =$

$a_n/2\pi r$, where a_n is a constant determined by the order of the Bessel function. If the weight $2\pi r g_{nl}(r)$ is increased for small r, the reflection will recede from the meridian. If $2\pi r g_{nl}(r)$ is increased for large r, the reflection will get close to the meridian.

From Eq. 3

$$w_{nl}(r) \equiv 2\pi r g_{nl}(r)$$

$$= q \int_0^{\infty} \int_0^{2\pi r} \rho_0'(r, \phi', z) \exp\{-i(n\phi'/r - 2\pi lz/c)\} d\phi' dz, \quad (7)$$

where $\phi' = r\phi$. The function $\rho_0'(r, \phi', z)$ represents a cylindrical section of one subunit at radius r expressed in the length of the circular arc instead of the angle involving the circular arc. Eq. 7 means that the weight $w_{nl}(r)$ is given by the Fourier transform of the cylindrical section with respect to the coordinates ϕ' and z. As an example, the Fourier transform for r equal to 23 Å is shown in Fig. 9 *a* on (n, l) plot (Klug et al., 1958). The weight $w_{nl}(r)$ is given by the value of the Fourier transform at the point (n, l). Because actin is elongated along the left-hand helix of pitch 59.8 Å shown by a straight dotted line in Fig. 9 *a*, the contour lines of the Fourier transforms are elongated perpendicularly to the dotted line. Therefore, $w_{-1,13}(23 \times 10^{-8}) \gg w_{1,15}(23 \times 10^{-8})$, and $w_{-1,13}(23 \times 10^{-8}) > w_{2,2}(23 \times 10^{-8})$ resulted. For correction of the model the shapes of actin on the cylindrical sections at various radial coordinates were so changed that the changes in $w_{-1,13}(r)$, $w_{1,15}(r)$, and $w_{2,2}(r)$ result in the desirable changes in the intensities and the positions of the reflections. Fig. 7 shows the final model obtained under the assumption that the shape of actin is nonpolar. The volume of actin is 5.54×10^4 Å^3, and gives a density of 1.23 g/cm^3 for the molecular weight of actin 42,000. The volume of the tropomyosin strand in one period is 1.77×10^5 Å^3, and gives a density of 1.26 g/cm^3 for the molecular weight of tropomyosin 67,000. In this model the actin subunits are elongated along the genetic helix, and those neighboring on the genetic helix are bonded together in the inner part of the filament, making the helix partly continuous.

The diffraction intensity and the cylindrically symmetrical difference Patterson function calculated for the new model are shown in Fig. 8. Fig. 8 *a* shows well the features of the diffraction pattern in question. The intensity on the 15th layer line and the positions of the intensity maxima on the 13th and 15th layer lines are well reproduced. The 2nd layer line is also reproduced at a good approximation. It is obvious on comparing Figs. 5 and 8 that the observed intensities are explained much better by the new model than the sphere model.

The characteristics of the shape of actin in the new model are reflected in $w_{-1,13}(r)$, $w_{1,15}(r)$, and $w_{2,2}(r)$, which were calculated for actin helix disregarding the small contribution from tropomyosin present in the range of r from 35 to 40 Å (Fig. 9). Because the genetic actin helix is approximately continuous in the inner part of the filament, the inner part makes little contributions to the 2nd and 15th layer lines, while it makes large contribution to the 13th layer line. Therefore, $w_{1,15}(r)$ and $w_{2,2}(r)$ are nearly equal to zero for $r \leq 20$ Å, while $w_{-1,13}(r)$ is large almost in the whole filament (Fig. 9 *b*). The weights $w_{1,15}(r)$ and $w_{2,2}(r)$ increase in the outer part. However, $w_{1,15}(r)$ is still $< w_{-1,13}(r)$ and $w_{2,2}(r)$, and $w_{2,2}(r)$ reaches

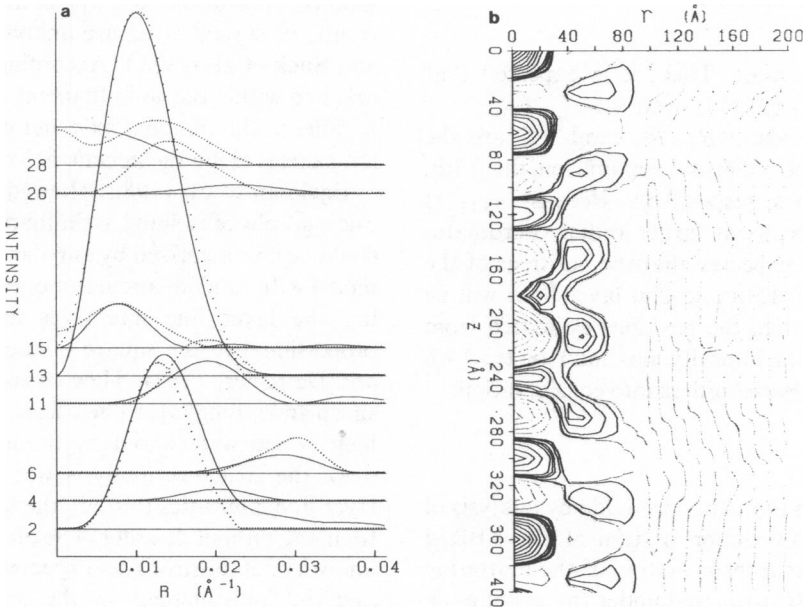

FIGURE 8 (*a*) Cylindrically averaged intensities calculated for the new model shown in Fig. 7 presented on a scale in which the maxima of the observed and calculated intensities are equal on the 13th layer line. The dotted lines (· · ·) show the observed intensities. (*b*) Cylindrically symmetrical difference Patterson function obtained by Fourier transformation of the calculated intensities of the new model shown in *a*. The same contour lines as in Fig. 3 *b* are used.

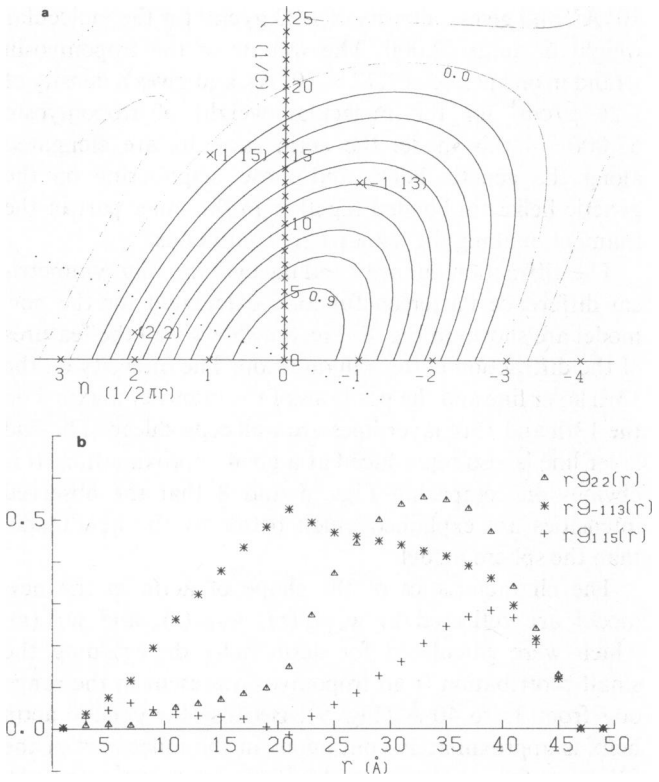

FIGURE 9 (*a*) Contour map of the Fourier transform of a cylindrical section at radius 23 Å shown in Fig. 7 *c*, that is, $w_{nl}(r) = 2\pi r g_{nl}(r)$ for r = 23 Å, presented on (n, l) plot. The peak at the origin was normalized to 1. The thick lines (—) are positive contour lines, and the thin lines (—) are zero and negative contour lines. Contour interval is 0.1. The dotted straight line (· · ·) passing through the origin shows a part of the continuous helix with a pitch of 59.8 Å on the cylindrical surface at radius 23 Å. (*b*) The weight $w_{nl}(r)$ for the 2nd, 13th, and 15th layer lines presented under the same normalization as in *a*.

$1.3 \times w_{-1,13}(r)$ at the most. Then, it is expected that $|G_{-1,13}(R_m)| \gg |G_{1,15}(R_m')|$, and $|G_{-1,13}(R_m)| > |G_{2,2}(R_m'')|$ will result, where R_m, R_m', and R_m'' are the radial coordinates of the intensity maxima on the 13th, 15th, and 2nd layer lines, respectively. Because $w_{1,15}(r)$ and $w_{2,2}(r)$ show the peaks at larger radial coordinates than $w_{-1,13}(r)$, it is also expected that the positions of the intensity maxima on the 15th and 2nd layer lines will be nearer to the meridian than the positions estimated from the radial coordinate of the intensity maximum on the 13th layer line by taking the Bessel orders into consideration.

SUMMARY

A new model of the thin filament was made by analysis of the small angle x-ray diffraction pattern of the ABRM involving inverse Fourier transformation of the scattering amplitude with the phase estimated under the assumption that the shape of actin is nonpolar. The new model explains well the features of the diffraction pattern concerning the reflections on the 13th, 15th, and 2nd layer lines.

Because the actin subunits are elongated along the genetic left-hand helix having a pitch of 59.8 Å, the helix appears rather like a continuous helix and the right-hand helices with pitches of 51.9 Å and 778 Å are made indistinct. Therefore, the reflection on the 13th layer line at the axial spacing of 59.8 Å is much stronger than the reflection on the 15th layer line at axial spacing 51.9 Å, although both are given by the first-order Bessel function and are comparable with each other in the height from the equator. Likewise, the reflection on the 2nd layer line corresponding to the second-order reflection from the helix with a pitch of 778 Å given by the second-order Bessel function is weaker than the reflection on the 13th layer line by more than the drop of the peak value of the Bessel function at the change of the order from the first to the second.

The continuous helixlike appearance of the genetic helix is enhanced in the inner part of the filament, where the actin subunits neighboring on the genetic helix are bonded together, partly making the helix really continuous. Therefore, the inner part makes very little contribution to the 2nd and 15th layer lines, while it makes a large contribution to the 13th layer line. For this reason, the position of the reflection is nearer to the meridian on the 15th layer line than the 13th layer line. Likewise, the reflection on the 2nd layer line is less distant radially from the reflection on the 13th layer line than estimated from the amount of peak shift brought about by alteration of the Bessel order from the first to the second.

The characteristics of the shape of actin clarified in this work are consistent with those that have been shown in the model of Wakabayashi et al. (1975) formed by the three-dimensional image reconstruction from the electron micrographs. The elongated shape of actin is in accord with the results of crystal structure analysis of Aebi et al. (1981) and Suck et al. (1981). According to Aebi et al., actin is oriented within the actin filament with its long axis roughly parallel to the filament axis, but our results show that the long axis is along the genetic helix.

Egelman et al. (1982) showed by analysis of electron micrographs of isolated actin filaments that the actin helix could be characterized by angular disorder, and proposed a model with random angular motions of the subunits affecting the layer line intensities and widths by a factor proportional to the square of the Bessel order (Egelman and DeRosier, 1982). They considered that the lack of a sharp and strong layer line corresponding to the half of the long period was caused by the angular disorder. In this work the structure analysis was done on the integrated layer line intensities to study the ideal structure of the thin filament without disorder. The intensity of the 381-Å layer line was not as strong as expected even after integration, and the indistinctness of the 381-Å layer line may be caused not only by the angular disorder but also by the shape of the actin subunit.

It was observed that the layer line became broader with the increase in the absolute value of the Bessel order, as

suggested by Egelman et al. (1982) and Egelman and DeRosier (1982), but there is one thing out of accord with their idea. The integral intensity of the 28th layer line has a peak on the meridian and off-meridional peaks (Fig. 3). The layer line is very sharp at the peak on the meridian, but it is as broad as the 13th layer line at the off-meridional peaks (Fig. 1), although no contributions other than that of the 0th order Bessel function are expected at the off-meridional peaks.

Under the assumption that the shape of actin is nonpolar, it is difficult to make the agreement between the observed and calculated intensities on the 2nd layer line better than shown in Fig. 8 *a*. It is also difficult to reproduce well the reflections at the large scattering angles; that is, on the 26th and 28th layer lines. For getting closer agreement between the observed and calculated intensities, it is necessary to introduce polarity to the shape of actin. The polarity can be introduced by deforming the shape of actin in the nonpolar model made in this work without missing the principal structural features so as to fill the difference between the observed and calculated intensities. By approximating the phase with that of the deformed model, inverse Fourier transformation of the scattering amplitude can be made again to form a polar model. The thin filaments show many layer-line reflections of indices higher than 28 in the range of the intermediate to high scattering angle (Lowy and Vibert, 1967; Namba et al., 1980). If they are involved in Fourier transformation to obtain the cylindrically symmetrical difference Patterson function of high resolution, the polarity of the shape of actin will be indicated in it, and information useful for making a polar model will be obtained. The work to make a polar model is in progress, and will be reported later.

We greatly appreciate Professor F. Oosawa, Dr. Y. Maeda, and Dr. S. Yoshino for recommending that we undertake the x-ray structure analysis of the ABRM, and for their guidance and helpful advice. We thank Dr. I. Sakurai, and members of his laboratory for help with densitometry of x-ray photographs. We also thank Dr. S. Amemiya for his help in acquiring muscles for the early stages of this work.

Received for publication 14 December 1982 and in final form 29 April 1983.

REFERENCES

Aebi, U., W. E. Fowler, G. Isenberg, T. D. Pollard, and P. R. Smith. 1981. Crystalline actin sheets: their structure and polymorphism. *J. Cell Biol.* 91:340–351.

Ebashi, S. 1972. Calcium ions and muscle contraction. *Nature (Lond.).* 240:217–218.

Egelman, E. H., N. Francis, and D. J. Derosier. 1982. F-actin is a helix with a random variable twist. *Nature (Lond.).* 298:131–135.

Egelman, E. H., and D. J. Derosier. 1982. The Fourier transform of actin and other helical systems with cumulative random angular disorder. *Acta Crystallogr. Sect. A. Cryst. Phys. Diffr. Theor. Gen. Crystallogr.* 38:796–799.

Elliott, G. E., and J. Lowy. 1968. Organization of actin in a mammalian smooth muscle. *Nature (Lond.).* 219:156–157.

Elzinga, M., J. H. Collins, W. M. Kuehl, and R. S. Adelstein. 1973. Complete amino-acid sequence of actin of rabbit skeletal muscle. *Proc. Natl. Acad. Sci. USA.* 70:2687–2691.

Hanson, J., and J. Lowy. 1963. The structure of F-actin and of actin filaments isolated from muscles. *J. Mol. Biol.* 6:46–60.

Haselgrove, J. C. 1972. X-ray evidence for a conformational change in the actin-containing filaments of vertebrate striated muscle. *Cold Spring Harbor Symp. Quant. Biol.* 37:341–352.

Jewell, B. R. 1959. The nature of the phasic and the tonic responses of the anterior byssal retractor muscle of Mytilus. *J. Physiol. (Lond.)* 149:154–177.

Klug, A., F. H. C. Krick, and H. W. Wyckoff. 1958. Diffraction by helical structures. *Acta Crystallogr.* 11:199–213.

Lehman, W., J. Kendrick-Jones, and A. G. Szent-Gyorgyi. 1972. Myosin-linked regulatory systems: comparative studies. *Cold Spring Harbor Symp. Quant. Biol.* 37:319–330.

Lowy, J., and B. M. Millman. 1963. The contractile mechanism of the anterior byssus retractor muscle of *Mytilus edulis. Phils. Trans. Roy. Soc. Lond. B Biol. Sci.* 246:105–148.

Lowy, J., and P. J. Vibert. 1967. Structure and organization of actin in a molluscan smooth muscle. *Nature (Lond.).* 215:1254–1255.

Lowy, J., and P. J. Vibert. 1972. Studies of the low-angle x-ray pattern of a molluscan smooth muscle during tonic contraction and rigor. *Cold Spring Harbor Symp. Quant. Biol.* 37:353–359.

Maeda, Y., I. Matsubara, and N. Yagi. 1979. Changes in thin filaments of crab striated muscle. *J. Mol. Biol.* 127:191–201.

Millman, R. M. 1964. Contraction in the opaque part of the adductor muscle of the oyster *(Crassostrea augulata). J. Physiol. (Lond.).* 173:238–262.

Namba, K., K. Wakabayashi, and T. Mitsui. 1980 X-ray structure analysis of the thin filament of crab striated muscle in the rigor state. *J. Mol. Biol.* 138:1–26.

Ohtsuki, I., T., Masaki, Y. Nonomura, and S. Ebashi. 1967. Periodic distribution of troponin along the thin filament. *J. Biochem. (Tokyo).* 61:817–819.

Sobieszek, A. 1973. The fine structure of the contractile apparatus of the anterior byssus retractor muscle of Mytilus edulis. *J. Ultrastruct. Res.* 43:313–343.

Squire, J. M. 1973. General model of myosin filament structure. III. Molecular packing arrangements in myosin filaments. *J. Mol. Biol.* 77:291–323.

Suck, D., W. Kabsch, and H. G. Mannherz. 1981. Three-dimensional structure of the complex of skeletal muscle actin and bovine pancreatic DNase I at 6-Å resolution. *Proc. Natl. Acad. Sci. USA.* 78:4319–4323.

Twarog, B. M. 1960. Effect of acetylcholine and 5-hydroxytriptamine on the contraction of a molluscan smooth muscle. *J. Physiol. (Lond.).* 152:236–242.

Vainshtein, B. K. 1966. Diffraction of X-Rays by Chain Molecules. Elsevier North-Holland, Inc., Amsterdam, London, and New York. 147–164.

Vibert, P. J., J. C. Haselgrove, J. Lowy, and F. R. Poulsen, 1972*a*. Structural changes in actin-containing filaments of muscle. *Nature, New Biology (Lond.).* 236:182–183.

Vibert, P. J., J. C. Haselgrove, J. Lowy, and F. R. Poulsen. 1972*b*. Structural changes in actin-containing filaments of muscle. *J. Mol. Biol.* 71:757–767.

Wakabayashi, T., H. E. Huxley, L. A. Amos and A. Klug. 1975. Three-dimensional image reconstruction of actin-tropomyosin complex and actin-tropomyosin-troponin T-troponin I complex. *J. Mol. Biol.* 93:477–497.

Woods, E. F. 1969. Comparative physicochemical studies on vertebrate tropomyosin. *Biochemistry.* 8:4336–4344.

Wray, J. S., P. J. Vibert, and C. Cohen. 1975. Diversity of cross-bridge configurations in invertebrate muscles. *Nature (Lond.).* 257:561–564.

Wray, J., P. J. Vibert, and C. Cohen. 1978. Actin filaments in muscle: pattern of myosin and tropomyosin/troponin attachments. *J. Mol. Biol.* 124:501–521.